Structure Parameter of Electrorheological Fluids in Shear Flow

ARTICLE *in* LANGMUIR · MAY 2011

Impact Factor: 4.46 · DOI: 10.1021/la2002018 · Source: PubMed

3 AUTHORS, INCLUDING:

Jile Jiang
National Institute of Metrology
14 PUBLICATIONS **140** CITATIONS
SEE PROFILE

Yonggang Meng
Tsinghua University
185 PUBLICATIONS **1,078** CITATIONS
SEE PROFILE

Langmuir

ARTICLE

pubs.acs.org/Langmuir

Structure Parameter of Electrorheological Fluids in Shear Flow

Jile Jiang, Yu Tian,* and Yonggang Meng

State Key Laboratory of Tribology, Tsinghua University, Beijing 100084, People's Republic of China

ABSTRACT: A structure parameter, $Sn = \eta_c\dot{\gamma}/\tau_E$, is proposed to represent the increase of effective viscosity due to the introduction of particles into a viscous liquid and to analyze the shear behavior of electrorheological (ER) fluids. Sn can divide the shear curves of ER fluids, τ/E^2 versus Sn, into three regimes, with two critical values Sn_c of about 10^{-4} and 10^{-2}, respectively. The two critical Sn_c are applicable to ER fluids with different particle volume fractions φ in a wide range of shear rate $\dot{\gamma}$ and electric field E. When $Sn < 10^{-4}$, the shear behavior of ER fluids is mainly dominated by E and by shear rate when $Sn > 10^{-2}$. The electric current of ER fluids under E varied with shear stress in the same or the opposite trend in different shear rate ranges. Sn_c also separates the conductivity variation of ER fluids into three regimes, corresponding to different structure evolutions. The change of Sn with particle volume fraction and E has also been discussed. The shear thickening in ER fluids can be characterized by $Sn_c(L)$ and $Sn_c(H)$ with a critical value about 10^{-6}. As an analogy to friction, the correspondence between τ/E^2 and friction coefficient, Sn and bearing numbers, as well as the similarity between the shear curve of ER fluids and the Stribeck curve of friction, indicate a possible friction origin in ER effect.

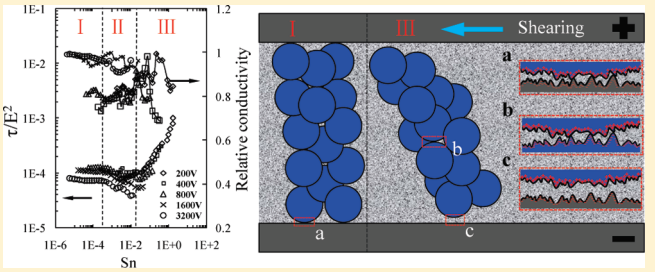

1. INTRODUCTION

Simple liquids generally behave as Newtonian liquids, of which viscosity is a constant and independent of the shear rate. When a certain amount of fine particles is introduced into a liquid, the viscosity of the suspension would generally increase. At a particle volume fraction of <5%, the Einstein equation can well describe the viscosity of the suspension. When the particle volume fraction increases to high values, the situation becomes more complex. The particle interaction may significantly affect the viscosity by altering the effective maximum packing fraction of the suspension.[1] For smart suspensions such as electrorheological (ER) fluids, the particle interactions can be instantly modulated by applying an external electric field E. This has attracted much attention in both scientific and engineering areas because of its abrupt and reversible rheological property change corresponding to the change of the applied E and its great potential in industrial applications, such as clutches, brakes, valves, and shock absorbers, since the discovery of electrorheology by Winslow in 1945.[2−4]

The reversible change of the rheological property in ER fluids is widely ascribed to the evolution of particle structures, such as columns in the form of body-centered tetragonal induced by the electric field strength E in a static state[5−14] and lamellae and stripes in shear flows when the applied E and the shear rate are both high enough.[15−18] The competitions among electrostatic force, hydrodynamic force, and thermal motion of particles are responsible for the structure evolutions inside ER fluids, which greatly affect the shear behaviors of ER fluids. Mason number,[19] $M_n = \eta_c\dot{\gamma}/2\varepsilon_0\varepsilon_f\beta^2E_0^2$, Peclet number, $Pe = 3\pi a^3\eta_c\dot{\gamma}/kT$, and $\lambda = \pi\varepsilon_0\varepsilon_c a^3\beta^2E_0^2/2kT$ present the relative importance of these forces in determining the structure and rheological property of ER fluids.[3] Although the structure evolution of ER fluids has been observed by the traditional and modern optical methods,[20−24] the structure effect on the shear strength of ER fluids has not been included in quantitative expressions yet.

Contact inside ER particles or between particles and electrodes also plays an important role in the ER effect.[25] Especially, the observed stick−slip behavior in the ER effect[26] has been directly ascribed to the friction inside the column of particles once the shear motion is applied under electric field. Enhancement of the interaction between electrodes and ER particles is also recently treated as an important way to improve the performance of ER fluids. Morphology modifications of electrodes in various ways[27−29] show stronger interactions between particles and electrodes to prevent a boundary slip at the ER/electrode interface. These results indicate that friction may play an important role in the ER effect, and the improvement of friction between electrodes and ER particles may result in a stronger ER effect. However, the mechanism of friction in the ER effect still needs further discussion.

To get an accurate control of the mechanical performance of an ER actuator, the relationship between the dynamic shear yield stress τ_y and the electric field strength E of ER fluids has been widely discussed and studied. Generally, $\tau_y \propto E^\alpha$, where $\alpha = 2$ in a polarization model[2,3] under a moderate voltage or $\alpha < 2$ in a conductivity model[30−32] under high voltages. In a scaling model τ_y is proportional to E^α, where $\alpha = 1.5$ or 2,[33] depending on the critical value of E. The variation of the exponent is related to both

Received: January 17, 2011
Revised: March 10, 2011
Published: April 13, 2011

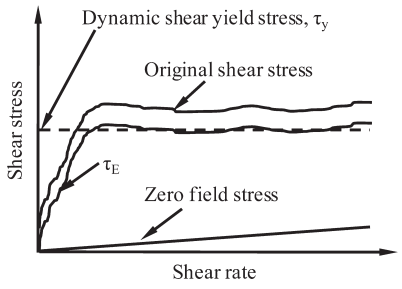

Figure 1. Schematic of the dynamic shear yield stress.

the electrostatic interaction strength between particles and particle chain structure evolutions under various conditions. The particle volume fraction φ is another important parameter that would significantly affect the chain aggregation and chain density for an ER fluid to provide a high shear yield stress. Generally, $\tau_y \propto \varphi^{\beta}$, where $\beta = 1$ in the single-chain model,[34−36] whereas $\beta = 1-2$ in different experimental results.[37] The problem becomes rather complex when the local particle volume fraction φ_c change[38,39] due to the chain structure evolution inside ER fluids under different E and shear rate is considered, so the relationship between φ and shear yield stress also needs further quantitative discussion.

Therefore, a parameter that could relate the structure evolutions to the applied electric field, the particle volume fraction, and the shear rate and that could indicate the friction effect would be very helpful to the further understanding of the ER mechanism. In this study, the rheological properties of ER fluids with different particle volume fractions of 5−30% were experimentally studied, accompanied with the electric current measurement. A parameter $\mathrm{Sn} = \eta_c\dot{\gamma}/\tau_E$ is proposed to analyze the shear behaviors of ER fluids with different shear rates, electric field strengths, and particle volume fractions. The variation in shear curves is ascribed to the structure evolutions and force competitions in ER effect. Sn is also normalized by $e^{\zeta\varphi}E^{\alpha}$ and shows a good agreement in a wide range of φ, E, and $\dot{\gamma}$. The friction between ER particles and that between ER particles and electrodes are also found to be strongly coupled with structure evolutions in the shear flow under electric field.

2. MATERIALS AND METHODS

The ER fluid used in the experiment was a mixture of zeolite particles and silicone oil. The zeolite particles (NaY, density = 1.8 g/cm^3, average diameter = 1 μm, purchased from Qilu Petroleum Corp., Shandong Province, People's Republic of China), added with 5 wt % glycerin as additives, were mixed with silicone oil (10 cSt at room temperature (20 °C), density = 0.93 g/cm^3, purchased from Beijing Chemical Corp., China) with nominal particle volume fractions of 5, 10, 15, 20, 25, and 30%, respectively. The details of the ER fluid preparation were introduced in our former work.[40] Glycerin used in this study is treated as one kind of polar molecule that can enhance the polarization ratio and the interaction force between ER particles.[41,42]

The rheological properties of the ER fluids were tested on a Physica MCR 301 rheometer (Anton Paar, Graz, Austria) equipped with a high-voltage power supply. The inner cylinder has a diameter $\Phi_i = 16.656$ mm, and the gap between the two concentric cylinders is $h = 0.714$ mm. A $6^1/_2$ digital multimeter (DM 3064, Rigol Corp., Beijing, China) was utilized to measure the current flowing through the ER fluids. All of the shearing tests were carried out at a temperature of 20 ± 0.1 °C controlled by the rheometer.

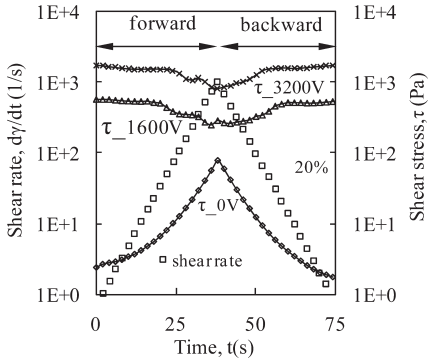

Figure 2. Typical response of the ER fluid under a fixed voltage (0, 1600, and 3200 V) and a logarithmically ramped shear rate.

Considering the definition of the shear yield stress of ER fluids by the Bingham model

$$\tau = \tau_E + \eta_c\dot{\gamma} \tag{1}$$

the dynamic shear yield stress, τ_y, is illustrated in Figure 1. η_c is the viscosity of the continuous phase in ER fluids. The residual value from the original shear stress under the applied voltage subtracting the zero field stress is regarded as τ_E, the stress contributed by the applied electric field. τ_y is the average value from the relatively stable part of the shear curve of τ_E with zero slope.

In each test, the voltage applied on the ER fluid was kept constant while the shear rate was increased and subsequently decreased logarithmically, as shown in Figure 2. The two processes were regarded as the forward mode and the backward mode, respectively.

3. RESULTS AND DISCUSSION

3.1. Shear Stress and Current . The typical results of the shearing test accompanied with electric current measurement in both the forward and backward modes are shown in Figure 3. Arrows indicate the change of shear rate in time sequence. As shown in Figure 3a, the current and shear stress changed in a similar tendency. According to the conduction model,[30] the current density J flowing through a single chain can be calculated as

$$J = \frac{3\varphi}{a^2}\int_0^a xj(x)\,\mathrm{d}x \tag{2}$$

where

$$j(x) = \sigma_f(0)\{(1-A) + A\exp[(E(x)/E_c)^{0.5}]\}E(x) \tag{3}$$

In eq 2, a is the particle diameter, and in eq 3 $\sigma_f(0)$ is the conductivity of the host fluid under zero electric field strength and $E(x)$ is the local electric field strength between particles. Because the particle interaction strength also depends on the local electric field, the current is expected to change with shear stress in the same trend and could be used to represent the two-particle interaction strength inside an ER fluid. However, the current slightly decreased with the increase of shear rate as shown in Figure 3a, whereas the shear stress decreased and then slightly increased at 49 s^{-1}. This shear stress increase can be observed until ER fluids with higher particle volume fraction φ are used as shown in Figure 3, panels b and c. Because the change of current and the shear stress contributed by the electrostatic interaction between particles should be in a similar trend, the shear stress

dx.doi.org/10.1021/la2002018 |Langmuir 2011, 27, 5814–5823

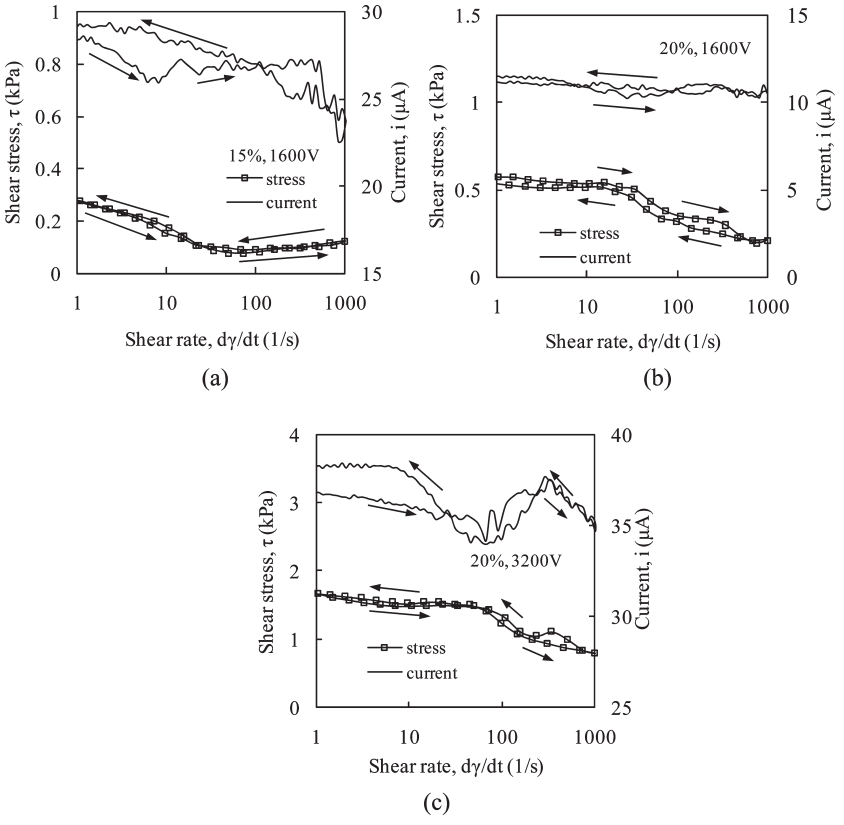

Figure 3. Current and shear stress of ER fluids under different voltages: (a) ER fluid of 15% particle volume fraction under 1600 V; (b) ER fluid of 20% particle volume fraction under 1600 V; (c) ER fluid of 20% particle volume fraction under 3200 V.

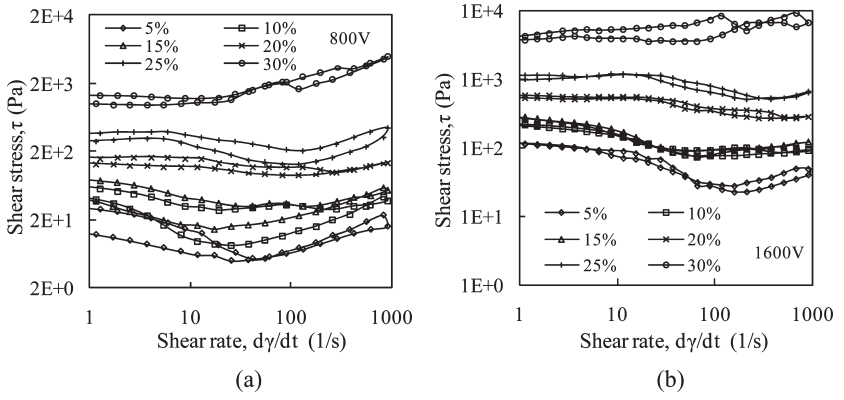

Figure 4. Shear stress of ER fluids in different particle volume fractions with shear rate ramped logarithmically from 1 to 1000 s^{-1} and then back to 1 s^{-1}: (a) under a fixed voltage of 800 V; (b) under a fixed voltage of 1600 V.

increase in Figure 3a can be ascribed to the enhancement of viscous contribution due to the increase of shear rate.

In Figure 3b, the current slightly increased around 90 s^{-1} while the shear stress decreased. This phenomenon is clearer in Figure 3c. It indicates an increase in the shear stress contributed by the electrostatic interaction between particles and a decrease of the viscous force due to the increase of shear rate. Under a fixed electric field E_0, a high shear rate would cause a high Mason number and a relatively weak ER effect[3,43] and lead to a decrease of shear stress as indicated in the low shear rate region, shown in Figure 3. With the increase of shear rate in a certain shear rate region, the particles in a relatively weak chain structure may be squeezed closer by the viscous force. Statistically, the average distance between the particles then decreased, leading to the enhancement of the local electric field strength between particles and the bulk current. However, with a further increase of shear rate, the viscous force is strong enough to affect the particle structures, and a decrease of electric current can be observed at high shear rate regions as shown in Figure 3, panels a and c.

3.2. ER Fluid with Different Particle Volume Fractions under the Same Electric Field. The shear curves of ER fluids with different particle volume fractions φ are shown in Figure 4. The forward and backward modes are both plotted. The shear stress changed in a nonmonotonous way. Taking the curve of

dx.doi.org/10.1021/la2002018 |*Langmuir* 2011, 27, 5814–5823

25% in Figure 4a as an example, the shear stress begins to decrease at 7 s^{-1} after a stable period and increased around 90 s^{-1}. In the backward mode, this phenonmenon occurred again. Both of the turning points were shifted to larger values when the particle volume fraction of ER fluids was increased. The turning points can be shifted to much larger values when higher voltages were applied. The phenonmenon can be observed over a wide range of shear rate and particle volume fraction according to our experimental results.

The shear thinning of ER fluids with high shear rate was suppressed when the 30% ER fluid was tested. As shown in Figure 4b, the shear stress remained around 5000 Pa at high shear rates, compared to the decrease of shear stress of ER fluid with smaller particle volume fractions of 5, 10, and 15% in the shear rate range of 10−100 s^{-1}. The decreasing trend of shear stress is alleviated in the shear rate range of 10−100 s^{-1} as the particle volume fraction increases. This indicates the structure of the ER fluid with a higher particle volume fraction has a stronger resistance to the shear flow.

As discussed in sections 3.1 and 3.2, the shear behavior of ER fluids in a wide shear rate range of 1−1000 s^{-1} with shear stress at 10^3 Pa varies in a complex way. The results of electric current proved the complex evolution of structures inside ER fluids. However, the classic characteristic number, such as the Mason number, can provide only one critical value to describe the phase transition in ER fluids.[3,19,43] The shift of the turning point indicates a possible relationship among the ER fluids with different volume fractions under shear flow, and the shear curve may be normalized by one parameter so as to reveal the mechanism of the ER effect. Therefore, a new characteristic number is needed to give a more proper description of the shear behaviors of ER fluids.

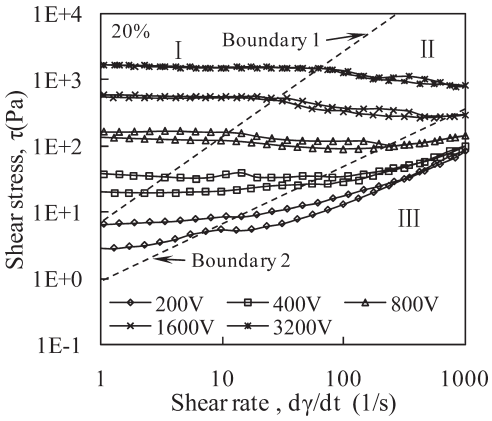

Figure 5. Regimes I, II, and III of shear curves of ER fluids with a particle volume fraction of 20% under voltages of 200−3200 V.

3.3. Structure Parameter. The shear behavior of ER fluid with a particle volume fraction φ of 20% under different voltages is shown in Figure 5. The shear stresses under these voltages all tended to decrease slightly and then to increase after going through a local minimum value. The very similar phenomenon can be observed in ER fluids with other particle volume fractions in our experiments and other different types of ER fluids in the former works: shear curves of ER fluids composed of laponite particles in silicone oil in 35.3 vol % by Parmar et al. shown in Figure 4a in ref 37; shear curves of ER fluids composed of DBSA-doped PANI-based particles in15 wt % by Kim et al. shown in Figure 3 in ref 44; shear curves of ER fluids composed of PANI/$BaTiO_3$ composite particles by Choi et al. shown in Figure 1b in ref 45; and shear curves of ER fluids composed of smooth Cr-doped titania particles in silicone oil in 10 vol % by Yin et al. shown in Figure 6b in ref 46. The similarity among these results indicates that Figure 5 shows a general phenomenon of ER fluids composed of different type particles and with different particle volume fractions.

In Figure 5, the shearing process of ER fluids was divided into three regimes, I, II, and III, with boundary 1 and boundary 2, respectively. It should be noted that the boundary does not have to be straight in a semilog plot. In Figure 6a, the shear stress τ is normalized by E as τ/E^2, and a structure parameter, $\mathrm{Sn} = \eta_c\dot{\gamma}/\tau_E$, is proposed. It expresses the effect of the viscosity of the fluids composed of ER particles and base oil with viscosity η_c in the shear flow under external electric field E. It includes the effects of particle volume fractions, which may decrease the average gap distance between particles, and results in a much higher real local shear rate of the viscous liquids and particle interactions, which may directly contribute to the shear stress. This dimensionless parameter also describes the relative importance of hydrodynamic force to shear resistance contributed by other factors, especially with the contribution of friction force. For the three different regimes, Sn_c corresponds to the point where shear curves intersect with boundaries.

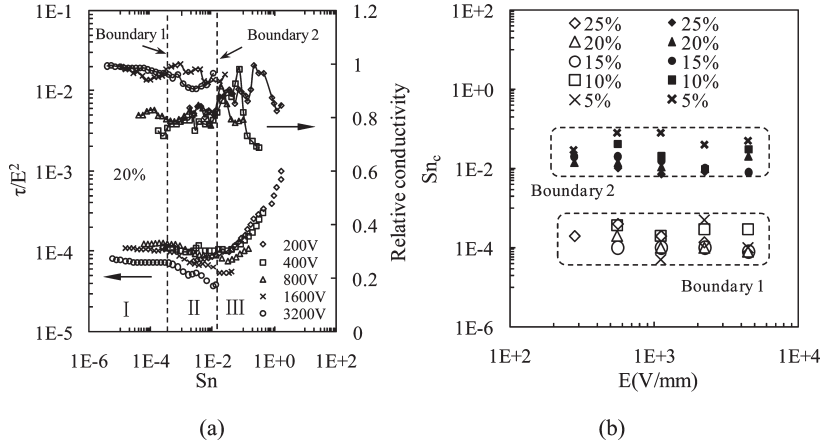

Figure 6. Sn_c of ER fluids: (a) relative conductivity and normalized shear stress versus Sn of an ER fluid with particle volume fraction of 20%; (b) with different particle volume fractions under different voltages.

dx.doi.org/10.1021/la2002018 |*Langmuir* 2011, 27, 5814–5823

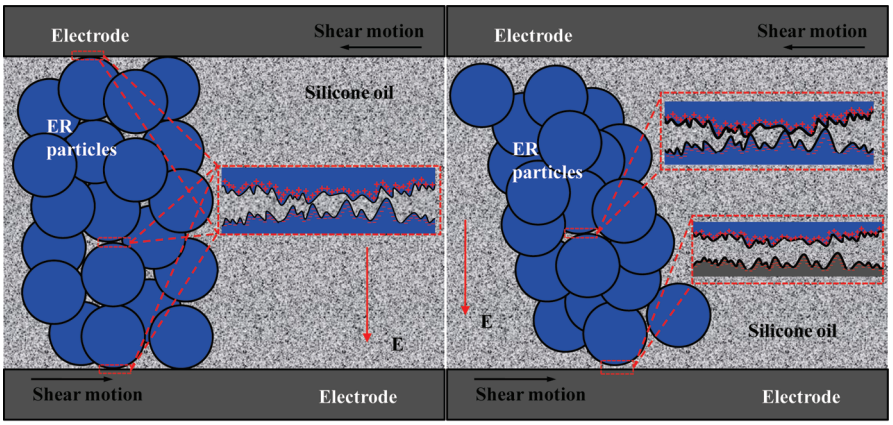

a. Regime I b. Regime III

Figure 7. Schematic of particle structures inside ER fluids in regimes I and III.

As shown in Figure 6a, the conductivity was calculated as $I/(SE)$, where I is the current and S is the area of the outer cylinder surface of the shear cell. The conductivity was normalized by the maximum value of each test. Sn_c values of ER fluids with different φ are plotted in Figure 6b. Sn_c values at boundary 1 are much smaller than the ones at boundary 2. The two sets of Sn_c distinguish the three different structure states inside ER fluids under different shear rates and different external electric field E. Below Sn_c at boundary 1, the normalized shear stress maintains a stable value when the structure of ER fluid is dominated by electrostatic force. After the Sn_c at boundary 2, the shear stress increases when the structure of ER fluids under electric fields is significantly affected by the high hydrodynamic force due to the applied high shear rate. In regime II, the hydrodynamic force due to the shear motion of base oil increases and the structures inside ER fluids evolve into relatively weaker ones. Therefore, regime II can be regarded as a transition regime. From regime I to regime III the relative conductivity behaves with more and more fluctuations, also distinguished by boundaries 1 and 2.

The attractive force between two particles, considered as hard and smooth spheres, is predicted by the Maxwell−Wagner polarization model[3] or the conduction model,[30] where the attractive force varies linearly with E^2. Then τ/E^2 can be treated as the ratio of a lateral force to a normal load, so τ/E^2 has a similar meaning to the friction coefficient. In $Sn = \eta_c\dot{\gamma}/\tau_E$, τ_E is the shear stress induced by the external electric field, as described in Figure 2. According to the real contact area between the particles or between particles and electrodes, as illustrated in Figure 7, τ_E may be affected more by the real normal stress P rather than the attractive force varying with E^2. From a microscopic point of view $\tau_E \propto P$. Hence, the curves shown in Figure 6a can be interpreted as an evolution of friction in ER fluids along with the shear motion.

In regime I, the normal force between particles and the one between particles and electrodes are decided by the electrostatic force, whereas the shear flow of the base oil has little effect on the structure of the particles, as shown in Figure 7a. The particles tended to align in lines spanning the space between the electrodes. Due to the limitation of the gap, the particles may get crowded in this dimension rather than the other two dimensions and initiate a normal load of electrodes/particles and particles/particles. Besides, the other part of the normal load of electrodes/particles and particles/particles is mainly contributed by the electrostatic interaction. Meanwhile, the strong friction among ER particles under the electric field will maintain the structure in the shear flow, so the strength of the structure inside ER fluids helps to maintain the normal load between particles and electrodes under the electric field, so as to obtain a high friction force transmitted between the counter electrodes. The shear resistance of the ER fluid thus can be mainly ascribed to the friction between the particles and the electrodes.

In regime III the shear stress curves under different voltages overlap with each other, as shown in Figure 6a. This phenomenon indicates that it is the hydrodynamic force determining the behavior of the ER fluids rather than the electric field. In this regime, the gap between the particles and the electrodes is formed and becomes larger due to the high shear rate, as shown in Figure 7b. The inner friction among particles under the electric field will be a benefit to maintaining a stronger structure, which will create the narrow path for the shear flow of base oil. In this situation, the shear behavior of the base oil will determine the shear behavior of the ER fluids and the force transmitted between electrodes. The surface morphology of the ER particles used in this study and reported in other works[3,21,46−48] is usually porous and rough. This property provides the fundamental strong friction among particles. In fact, the new structure parameter proposed in this work is in a similar form to the bearing number $\eta V/P$ in the Stribeck curve widely used in tribology,[49,50] in which η is the viscosity of the lubricant, V is the relative velocity, and P is the applied pressure or normal load. The bearing number is a typical parameter used to clarify different lubrication regimes.

In regime I the structure inside ER suspensions is determined by the applied electric field, and the particles attach to each other firmly due to the strong polarization attraction. The relative motion is weak, so the current is rather smooth. In regime III the motion of ER particles is strongly affected by the shear flow. The particles at the edge of the stripes experience more turbulence from viscous force in shear flow despite the formation of thick stripes. This may modify the contact between the particle and the electrode and then lead to a large variation of the local conductivity.

The schematic structure inside ER fluids in regimes I and III shown in Figure 7 can be considered as the normal states in ER

dx.doi.org/10.1021/la2002018 |*Langmuir* 2011, 27, 5814–5823

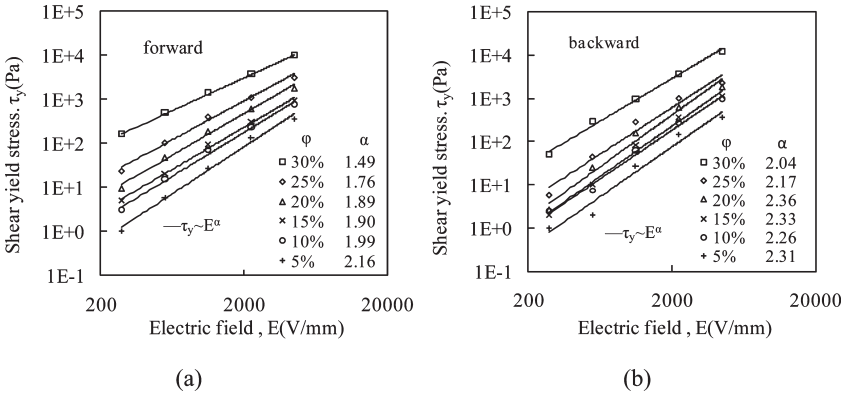

Figure 8. Shear yield stress of ER fluids with different particle volume fractions φ under different voltages, fitted by E^{α}: (a) data in forward mode; (b) data in backward mode.

fluids. The particle structure of ER fluids gradually evolves from regime I to regime III. The ER fluids with low particle volume fraction and low electric field have no clear Sn_c at boundary 1. The ER fluid with φ of 30% has no clear Sn_c at either boundary 1 or boundary 2. Because the structure inside ER fluids with lower particle volume fraction is more easily affected by the shear motion, the shear behavior determined by electrostatic force is weak. On the contrary, a stronger particle structure can be more easily obtained in the ER fluid with φ of 30%, so the shear curve under a shear rate of 10−1000 s^{-1} has no great change.

The three regimes clarified by the proposed structure parameter Sn may reflect the role of friction in ER effect and the transition of friction during the shear flow. These regimes might be determined by the condition of friction between particles and electrodes or among particles. From this point of view, Sn concerns friction more than the general electrostatic interaction consideration. Flow curves can be described by another three regions: preyield, yield, and past yield regions. It is well-known that the interaction among particles in ER fluids can be verified as electrostatic, van der Waals, hydrolubrication, and repulsive steric forces. Friction is only one type of interaction among the ER particles. Flow curves described by the proposed Sn indicate the friction origin in the shear strength of ER fluids. An appropriate modification of Sn is necessary to cover other flow curves and to be of great help to comprehensively understand the ER effect.

According to the proposed structure parameter, the dynamic shear yield stress of ER fluids is selected when $Sn < 10^{-4}$. In this period the shear behavior is dominated by the electric field rather than the shear rate. The shear curves in this period are also relatively stable, which agrees with the classic definition of dynamic yield stress. The influence of electric field E and particle volume fraction φ on dynamic shear yield stress of ER fluids is discussed in the following.

3.4. Relationship between Shear Yield Stress and Electric Field as $\tau_y \propto E^{\alpha}$. In the forward mode, α decreases with the increase of φ as shown in Figure 8a. The decrease of α indicates that the effect of E on shear yield stress of ER fluids with a lower φ is more significant. The ER particles are attached with some net charges when they are mixed with base oil and applied external electric field. These polarized particles will be driven to the electrode and then back to the counter electrode once it contacts the electrode and gets some opposite net charges. This kind of movement between electrodes will be suppressed by the shear flow, and it is considered as one kind of contribution to the increase of the viscosity.[3] When the particle concentration increases, this kind of motion will be suppressed, and its contribution to the shear stress under the same electric field will be reduced, leading to a smaller exponent of E.

In the backward mode test, exponents of E at different φ of ER fluids are similar to each other as shown in Figure 8b. The average value of α is greater than that in the forward mode. As described previously, the forward mode is followed by the backward mode in a single test. We think that the stripe structure preformed and stretched in the backward mode may result in a stronger ER effect, showing that the shear history has an important influence on the rheological performance of ER fluids.

3.5. Relationship between Normalized Shear Yield Stress and Particle Volume Fraction as $\tau_y/E^{\alpha} \propto e^{\zeta\varphi}$. The dynamic shear yield stress normalized by E^{α} was fitted by $e^{\zeta\varphi}$ as shown in Figure 9. The exponent α is taken from Figure 8. ζ, the slope of φ, is plotted versus the applied voltage in the inset figure. In the forward mode, ζ is 0.31 ± 0.01 in the whole range of the applied voltage, whereas in the backward mode, ζ is 0.20 ± 0.01 except for β = 0.224 under 400 V. The shear yield stress can be determined by the electric field E and the particle volume fraction φ as

$$\tau_y \propto e^{\zeta\varphi} E^{\alpha} \tag{4}$$

The experimental results show that the normalized dynamic shear yield stress increases exponentially with the particle volume fraction of ER fluids, with an exponent influenced by the shear history. The smaller τ_y/E^{α} in the backward mode can be ascribed to the larger α, shown in Figure 8b, indicating that the preshearing has already initiated regular structures, resulting in a larger shear yield stress of ER fluids in the backward mode than in the forward mode.

The viscosity of hard sphere colloidal suspensions is described as a polynomial function of the particle volume fraction φ.[51] The dynamic shear yield stress of MR fluid is scaled as φ^{ζ}, in which ζ = 0.8−1.4.[36] ζ = 2 and 3 was experimentally discovered for a discotic clay gel.[52] ζ = 1 was confirmed both in the condition when the shear strain exceeds a critical value[39] and when the electrical torque and the chain orientation angle were taken into consideration.[53,54] For MR fluids, the shear yield stress generally scales with the particle volume fraction linearly.[55−57] ζ is different according to different materials and different test mode.

dx.doi.org/10.1021/la2002018 |*Langmuir* 2011, 27, 5814–5823

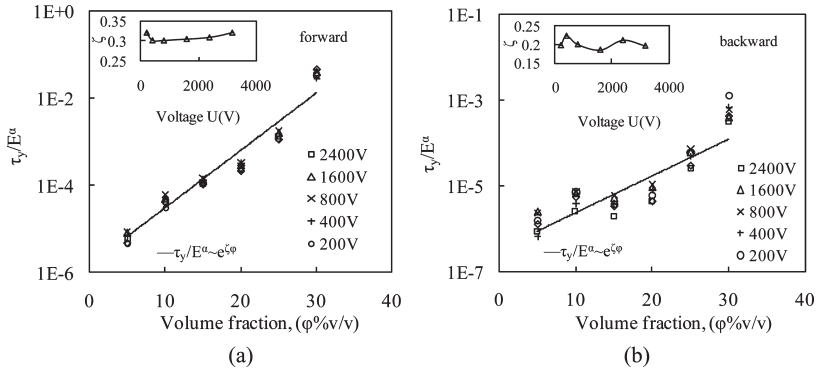

Figure 9. Shear yield stress normalized by E^{α} with α at different particle volume fractions. (a) data in forward mode; (b) data in backward mode. The slope of the exponent in $e^{\zeta\varphi}$ is shown in the inset with voltages of 0−3200 V.

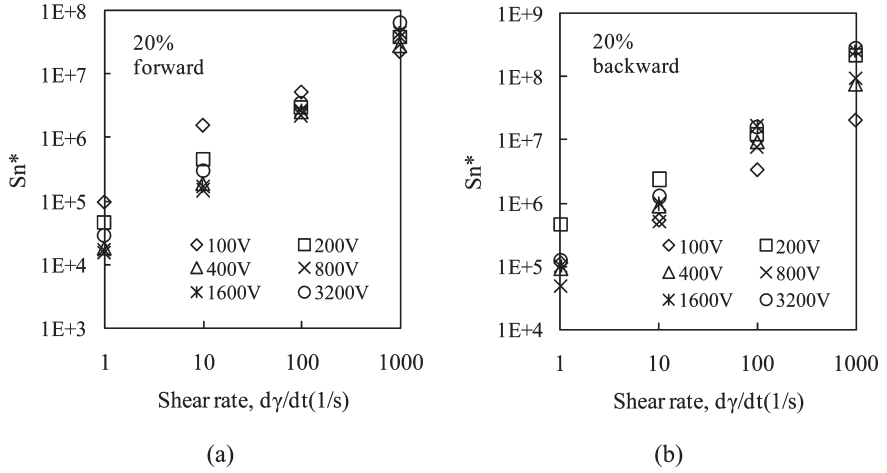

Figure 10. Normalized Sn of 20% ER fluid in forward (a) and backward (b) mode under different electric fields.

And usually one ζ is not suitable for other conditions. Different ζ in φ^{ζ} are also proposed according to different chain models and experimental results. The physical meaning of this power law is generally explained by a single-chain model when ζ = 1, but in the real shear flow, the single-chain model is obviously not a good model to describe the complicated shear behavior. The power function, φ^{ζ}, no matter the exponent, can be regarded as the several initial terms of the Taylor series expansion of $e^{\zeta\varphi}$ as

$$e^{\zeta\varphi} = \sum_{i=0}^{\infty} \frac{\zeta^i}{i!} \varphi^i \qquad (5)$$

except for the constant value of 1, which can be treated as a constant coefficient relating to the influence of the structure evolution of ER fluids. The higher terms in Taylor series of $\exp(\zeta\varphi)$ can be neglected because of the smaller numerator ζ^i and the larger denominator $n!$. ζ indicates the impact of the nominal particle volume fraction to the shear yield stress. Here, the form of $e^{\zeta\varphi}$ is proved to be more reasonable throughout a wide range of shear rate and shear stress according to our experiment results. The form of $e^{\zeta\varphi}$ provides one method to consider the complex chain structures by the sum of φ^{ζ} in the form of exponential function. The physical meaning of this sum may lead to further discussions and be beneficial to the understanding of the structure of ER particles under electric fields.

3.6. Normalized Sn. According to Figure 1 and the two constants obtained in sections 3.4 and 3.5, Sn can be normalized by $Sn^* = Sn \cdot E^{\alpha} \cdot e^{\zeta\varphi}$, and the results are shown in Figure 10. According to the definition of $Sn = \eta_c\dot{\gamma}/\tau_E$, Sn* can describe the contribution of viscosity of base oil to the whole ER effect. It scales with shear rate in the same slope in both forward and backward mode because of the same base oil used. Most Sn* in the backward mode are larger than the values in the forward mode, as shown in Figures 10 and 11. Considering the strong structures formed in the backward mode due to the preshearing in the forward mode, the actual gap for the shear flow of oil is smaller in the backward mode, so ER fluids can provide a larger shear resistance. The Sn* of ER fluids with different φ agrees with others except for the one of 30%, which is slightly below the average value. In Figure 9 the stress of 30% ER fluid is higher than the value predict by $e^{\zeta\varphi}$, so in Figure 11 $Sn^* = Sn \cdot E^{\alpha} \cdot e^{\zeta\varphi}$ will not be as high as expected when φ is 30%.

3.7. Sn in Shear Thickening of ER Fluids. The shear thickening of electrorheological and magnetorheological fluids above a certain low critical shear rate and high critical electric/magnetic field strength has been reported recently.[58,59] The friction is considered as playing an important role in the origin of the shear resistance of ER fluids. The details of different test modes and measurements of different types of ER fluids have been reported in refs 58 and 59. This kind of sudden change in shear stress can also be found in the reports of other

dx.doi.org/10.1021/la2002018 |*Langmuir* 2011, 27, 5814–5823

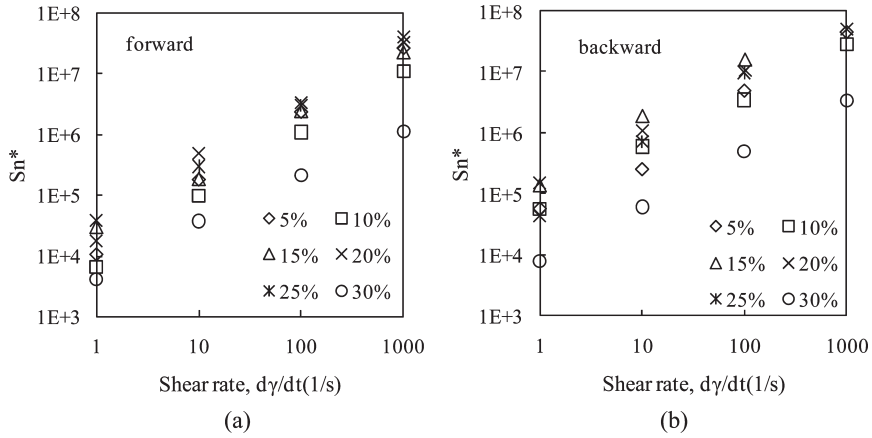

Figure 11. Average normalized Sn under the same shear rate of different particle volume fractions in forward (a) and backward (b) mode.

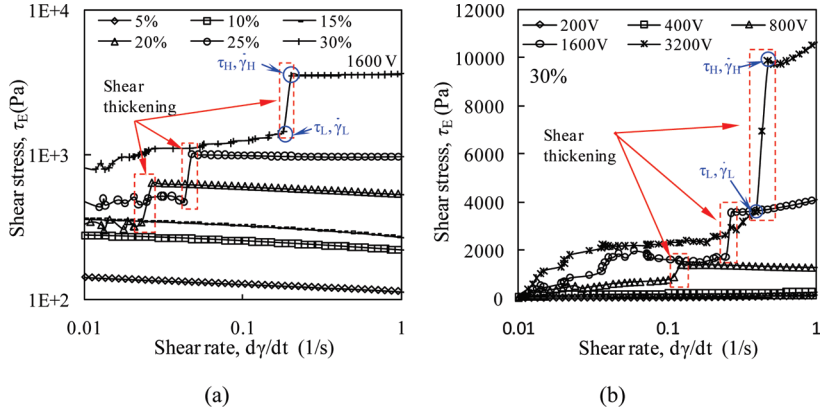

Figure 12. Shear thickening of ER fluids: (a) ER fluids of different particle volume fractions under the same voltage of 1600 V; (b) ER fluid with particle volume fraction of 30% under different voltages of 200−3200 V.

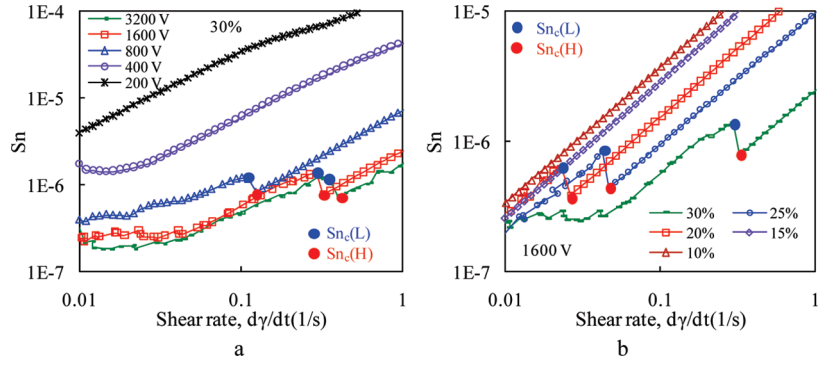

Figure 13. Sn of ER fluids when shear thickening happens: (a) Sn of ER fluids with different particle volume fractions under a voltage of 1600 V; (b) Sn of ER fluid with particle volume fraction of 30% under voltages of 200−3200 V.

researchers,[46,60] although different ER materials and test protocols were used. The shear curves of the ER fluids with different particle volume fractions under the same voltage of 1600 V are shown in Figure 12a. The shear curves of an ER fluid with particle volume fraction of 30% under different voltages of 200−3200 V are shown in Figure 12b. The shear stress shown in Figure 12 is obtained by eq 1. Under the same voltage, the shear thickening phenomenon can be triggered more easily in an ER fluid with a higher particle volume fraction. With the increase of the external electric field, the increment of the shear stress with the onset of the shear thickening becomes larger. The critical shear rate beyond which the shear thickening happens is also shifted to a higher value when the particle volume fraction or the applied voltage increases.

The structure parameter Sn of the shear curves in Figure 12 is presented in Figure 13. It shows that Sn values of the shear thickening points of ER fluid of 30% under different voltages agree with each other around 10^{-6} with small discrepancy, whereas the Sn of the shear thickening point increases slightly

dx.doi.org/10.1021/la2002018 |*Langmuir* 2011, 27, 5814–5823

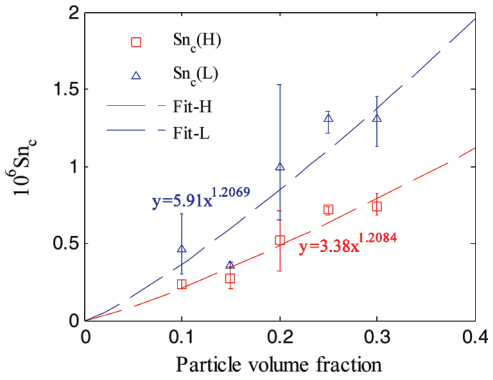

Figure 14. Critical structure parameters $Sn_c(H)$ and $Sn_c(L)$ of different particle volume fractions under different voltages 800−5600 V fit by $y = ax^b$, respectively.

with the increase of particle volume fraction under the same voltage. We define the critical structure parameter $Sn_c(H) = \eta_c\dot{\gamma}_H/\tau_H$ and $Sn_c(L) = \eta_c\dot{\gamma}_L/\tau_L$, in which $\dot{\gamma}_L$, τ_L, $\dot{\gamma}_H$, and τ_H are illustrated in Figure 12. $Sn_c(L)$ represents the point right before the shear thickening, whereas $Sn_c(H)$ represents the point where the shear thickening just happens. Both $Sn_c(L)$ and $Sn_c(H)$ of ER fluids with different particle volume fractions and applied voltages are shown in Figure 14. The critical structure parameters increase with particle volume fraction in the form of $y = ax^b$ for both $Sn_c(L)$ and $Sn_c(H)$ with an exponent of about $b = 1.2$ but with different factor ratios of 5.91 and 3.38.

Shear thickening happens before regimes II and III as discussed above. The single particle chain structure can be regarded as a major structure type when the small shear rate is applied around 0.01 s^{-1}. The particles in a single chain cannot fit into each other well to perfectly align in a straight line because of the limitation of the gap between the electrodes along electric field. As the shear rate increases gradually, the shear flow will cause the two neighbor chains to jam and initiate relocations of ER particles, resulting in an increase of shear resistance. This shear thickening is a result of competition between the shear contributed viscous force and the electrostatic force between particles.

4. CONCLUSIONS

Structure evolutions under different voltages and shear rates determine the behaviors of shear stress and electric current of ER fluids. The current can be treated as a reference parameter to study the structure evolution inside the ER fluids. Along with the current test, a new structure parameter Sn is proposed and verified to effectively describe the structure evolution of the ER fluids, including the newly discovered phenomenon of shear thickening. The structure evolution can be distinguished by three critical numbers, 10^{-6}, 10^{-4}, and 10^{-2} of Sn. Analysis of Sn indicates that friction plays important roles in the shear behavior of ER fluids. The dynamic shear yield stress of ER fluid is treated as a function of particle volume fraction φ and the electric field intensity E in terms of $e^{\zeta\varphi}E^{\alpha}$. α and ζ are relatively stable with respect to the particle volume fractions but influenced by the shear history of ER fluids.

AUTHOR INFORMATION

Corresponding Author

*Fax: 86-10-62781379. Phone:86-10-62782981. E-mail: tianyu@mail.tsinghua.edu.cn.

ACKNOWLEDGMENT

This work is sponsored by the National Basic Research Program of China with Grant 2011CB707603 and by the National Natural Science Foundation of China with Grants 50875152 and 51021064.

REFERENCES

(1) Mueller, S.; Llewellin, E. W.; Mader, H. M. *Proc. R. Soc. London, A* **2010**, *466*, 1201–1228.
(2) Winslow, W. M. *J. Appl. Phys.* **1949**, *20*, 1137–1140.
(3) Parthasarathy, M.; Klingenberg, D. J. *Mater. Sci. Eng. Res.* **1996**, *17*, 57–103.
(4) Tian, Y.; Meng, Y. G.; Mao, H. R.; Wen, S. Z. *J. Appl. Phys.* **2002**, *92*, 6875–6879.
(5) Tao, R.; Jiang, Q. *Phys. Rev. Lett.* **1994**, *73*, 205–208.
(6) Tian, Y.; Wen, S. Z.; Meng, Y. G. *Phys. Rev. E* **2003**, *67*, 051501.
(7) Tao, R.; Jiang, Q. *Phys. Rev. E* **1998**, *57*, 5761–5765.
(8) Gulley, G. L.; Tao, R. *Phys. Rev. E* **1997**, *56*, 4328–4336.
(9) Tao, R.; Sun, J. M. *Phys. Rev. Lett.* **1991**, *67*, 398–401.
(10) See, H. *J. Phys. D—Appl. Phys.* **2000**, *33*, 1625–1633.
(11) Gao, X. Y.; Zhao, X. P.; Zheng, C. Q. *J. Phys. D* **1998**, *31*, 3397–3402.
(12) Ma, H. R.; Wen, W. J.; Tam, W. Y.; Sheng, P. *Adv. Phys.* **2003**, *52*, 343–383.
(13) Hao, T.; Kawai, A.; Ikazaki, F. *Langmuir* **1999**, *15*, 918–921.
(14) Hao, T.; Kawai, A.; Ikazaki, F. *Langmuir* **2000**, *16*, 3058–3066.
(15) Tian, Y.; Li, C. H.; Zhang, M. L.; Meng, Y. G.; Wen, S. Z. *J. Colloid Interface Sci.* **2005**, *288*, 290–297.
(16) Bossis, G.; Lemaire, E.; Volkova, O.; Clercx, H. *J. Rheol.* **1997**, *41*, 687–704.
(17) Volkova, O.; Cutillas, S.; Bossis, G. *Phys. Rev. Lett.* **1999**, *82*, 233–236.
(18) Cao, J. G.; Huang, J. P.; Zhou, L. W. *J. Phys. Chem. B* **2006**, *110*, 11635–11639.
(19) Marshall, L.; Zukoski, C. F.; Goodwin, J. W. *J. Chem. Soc., Faraday Trans 1* **1989**, *85*, 2785–2795.
(20) Shen, M.; Cao, J. G.; Xue, H. T.; Huang, J. P.; Zhou, L. W. *Chem. Phys. Lett.* **2006**, *423*, 165–169.
(21) Wen, W. J.; Huang, X. X.; Yang, S. H.; Lu, K. Q.; Sheng, P. *Nat. Mater.* **2003**, *2*, 727–730.
(22) Bossis, G.; Metayer, C.; Zubarev, A. *Phys. Rev. E* **2007**, *76*, 041401.
(23) Martin, J. E.; Odinek, J.; Halsey, T. C. *Phys. Rev. Lett.* **1992**, *69*, 1524–1527.
(24) Chen, T. J.; Zitter, R. N.; Tao, R. *Phys. Rev. Lett.* **1992**, *68*, 2555–2558.
(25) Bonnecaze, R. T.; Brady, J. F. *J. Chem. Phys.* **1992**, *96*, 2183–2202.
(26) Woestman, J. T. *Phys. Rev. E* **1993**, *47*, 2942–2945.
(27) Liu, L. Y.; Huang, X. X.; Shen, C.; Liu, Z. Y.; Shi, J.; Wen, W. J.; Sheng, P. *Appl. Phys. Lett.* **2005**, *87*, 104106.
(28) Wang, X. Z.; Shen, R.; Wang, D.; Lu, Y.; Lu, K. Q. *Mater. Des.* **2009**, *30*, 4521–4524.
(29) Wang, X. Z.; Shen, R.; Sun, G.; Wen, W. J.; Lu, K. Q. *Int. J. Mod. Phys. B* **2007**, *21*, 4940–4944.
(30) Wu, C. W.; Conrad, H. *J. Phys. D—Appl. Phys.* **1996**, *29*, 3147–3153.
(31) Davis, L. C. *J. Appl. Phys.* **1997**, *81*, 1985–1991.
(32) Wu, C. W.; Conrad, H. *Phys. Rev. E* **1997**, *56*, 5789–5797.
(33) Choi, H. J.; Cho, M. S.; Kim, J. W.; Kim, C. A.; Jhon, M. S. *Appl. Phys. Lett.* **2001**, *78*, 3806–3808.
(34) Shkel, Y. M.; Klingenberg, D. J. *J. Rheol.* **1999**, *43*, 1307–1322.
(35) Martin, J. E.; Anderson, R. A. *J. Chem. Phys.* **1996**, *104*, 4814–4827.
(36) Kuzhir, P.; Lopez-Lopez, M. T.; Bossis, G. *J. Rheol.* **2009**, *53*, 127–151.

(37) Parmar, K. P. S.; Meheust, Y.; Schjelderupsen, B.; Fossum, J. O. *Langmuir* **2008**, *24*, 1814–1822.
(38) von Pfeil, K.; Graham, M. D.; Klingenberg, D. J.; Morris, J. F. *J. Appl. Phys.* **2003**, *93*, 5769–5779.
(39) Klingenberg, D. J.; Zukoski, C. F. *Langmuir* **1990**, *6*, 15–24.
(40) Tian, Y.; Meng, Y. G.; Wen, S. Z. *J. Appl. Phys.* **2001**, *90*, 493–496.
(41) Shen, R.; Wang, X. Z.; Lu, Y.; Wang, D.; Sun, G.; Cao, Z. X.; Lu, K. Q. *Adv. Mater.* **2009**, *21*, 4631–4635.
(42) Shen, R.; Wang, X. Z.; Lu, Y.; Wen, W. J.; Sun, G.; Lu, K. Q. *J. Appl. Phys.* **2007**, *102*, 024106.
(43) Kittipoomwong, D.; Daniel, J.; Shkel, Y. M.; Morris, J. F.; Ulicny, J. C. *J. Rheol.* **2008**, *52*, 225–241.
(44) Kim, S. G.; Lim, J. Y.; Sung, J. H.; Choi, H. J.; Seo, Y. *Polymer* **2007**, *48*, 6622–6631.
(45) Choi, H. J.; Jhon, M. S. *Soft Matter* **2009**, *5*, 1562–1567.
(46) Yin, J. B.; Zhao, X. P.; Xiang, L. Q.; Xia, X.; Zhang, Z. S. *Soft Matter* **2009**, *5*, 4687–4697.
(47) Hong, J. Y.; Choi, M.; Kim, C.; Jang, J. *J. Colloid Interface Sci.* **2010**, *347*, 177–182.
(48) Cao, J. G.; Shen, M.; Zhou, L. W. *J. Solid State Chem.* **2006**, *179*, 1565–1568.
(49) Moshkovich, A.; Perfilyev, V.; Lapsker, I.; Rapoport, L. *Tribol. Lett.* **2010**, *37*, 645–653.
(50) Kalin, M.; Velkavrh, I.; Vizintin, J. *Wear* **2009**, *267*, 1232–1240.
(51) Dekruif, C. G.; Vanlersel, E. M. F.; Vrij, A.; Russel, W. B. *J. Chem. Phys.* **1985**, *83*, 4717–4725.
(52) Pignon, F.; Piau, J. M.; Magnin, A. *Phys. Rev. Lett.* **1996**, *76*, 4857–4860.
(53) Martin, J. E.; Odinek, J.; Halsey, T. C.; Kamien, R. *Phys. Rev. E* **1998**, *57*, 756–775.
(54) Anderson, R. A. *Langmuir* **1994**, *10*, 2917–2928.
(55) Bell, R. C.; Karli, J. O.; Vavreck, A. N.; Zimmerman, D. T.; Ngatu, G. T.; Wereley, N. M. *Smart Mater. Struct.* **2008**, *17*, 015028.
(56) Bossis, G.; Lacis, S.; Meunier, A.; Volkova, O. *J. Magn. Magn. Mater.* **2002**, *252*, 224–228.
(57) Shkel, Y. M.; Klingenberg, D. J. *J. Rheol.* **2001**, *45*, 351–368.
(58) Tian, Y.; Jiang, J. L.; Meng, Y. G.; Wen, S. Z. *Appl. Phys. Lett.* **2010**, *97*, 151904.
(59) Tian, Y.; Zhang, M. L.; Jiang, J. L.; Pesika, N.; Zeng, H. B.; Israelachvili, J. N.; Meng, Y. G.; Wen, S. Z. *Phys. Rev. E* **2010**, *83*, 011401.
(60) Ramos-Tejada, M. M.; Espin, M. J.; Perea, R.; Delgado, A. V. *J. Non-Newtonian Fluid Mech.* **2009**, *159*, 34–40.